Paper
Int'l J. of Aeronautical & Space Sci. 17(2), 149–156 (2016)
DOI: http://dx.doi.org/10.5139/IJASS.2016.17.2.149

IJASS
International Journal of Aeronautical and Space Sciences

Flow Field Analysis on the Stagnation Streamline of a Blunt Body

Chang-Ho Lee*

Aerodynamics Research Team, Korea Aerospace Research Institute, Daejeon 34133, Republic of Korea

Abstract

The hypersonic flow on the stagnation streamline of a blunt body is analyzed with quasi one-dimensional (1-D) Navier-Stokes equations approximated by adopting the local similarity to the two-dimensional (2-D)/axisymmetric Navier-Stokes equations. The governing equations are solved using the implicit finite volume method. The computational domain is confined from the stagnation point to the shock wave, and the shock fitting method is used to find the shock position. We propose a boundary condition at the shock, which employs the shock wave angle in the vicinity of the stagnation streamline using the shock shape correlation. As a result of numerical computation conducted for the hypersonic flow over a sphere, the proposed boundary condition is shown to improve the accuracy of the prediction of the shock standoff distance. The quasi 1-D Navier-Stokes code is efficient in computing time and is reliable for the flow analysis along the stagnation streamline and the prediction of heat flux at the stagnation point in the hypersonic blunt body flow.

Key words: Hypersonic Flow, Blunt Body, Stagnation Streamline, Heat Flux

1. Introduction

Flow field analysis around the nose tip and leading edge of the hypersonic vehicle has attracted much interest because the largest heat flux occurs in these regions. The Fay and Riddell formula [1], which is the correlation of numerical solutions of boundary layer equations, obtains the heat flux at the stagnation point of a blunt body and is still used today for quick analysis. After the success of Moretti and Abbett's [2] work, computational fluid dynamics has progressed rapidly and is used widely in solving hypersonic blunt body flows. Fig. 1 shows a schematic of the hypersonic flow around a blunt body. In the typical approach to solving this flow, the computational domain should cover the subsonic region in the shock layer to ensure that the flow at the outflow boundary is supersonic. Therefore, although the stagnation properties are needed, we have to solve the two-dimensional (2-D) domain. On the other hand, if the flow equations on the stagnation streamline can be solved, the computational time might be significantly reduced. Several researchers have attempted to solve the flow field along the stagnation streamline of a blunt body in supersonic and hypersonic flows. Kao [3] considered flow analysis near the stagnation streamline of a blunt body by applying local similarity to the 2-D Navier-Stokes equations in a rarefied flow. Jain and Adimurthy [4] investigated the flow structure of a merged layer near the stagnation point of a blunt body for flights in a rarefied atmosphere by solving Navier-Stokes

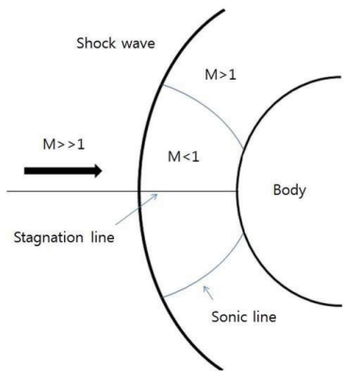

Fig. 1. Hypersonic flow around a blunt body.

* Principal Researcher, Corresponding author: leech@kari.re.kr

Received: August 25, 2015 Revised: March 3, 2016 Accepted: May 12, 2016

http://ijass.org pISSN: 2093-274x eISSN: 2093-2480

equations, adopting the concept of local similarity. These researches only considered flight conditions with very small Reynolds numbers in rarefied flow. The study by Klomfass and Müller [5] was the first attempt to adopt modern computational fluid dynamics algorithms to solve the conservative form of dimensionally reduced Navier-Stokes equations approximated by Kao [3]. An implicit finite volume algorithm using the shock fitting method was applied to solve the equations. Also, William et al. [6] adopted the shock capturing method to solve quasi one-dimensional (1-D) Navier-Stokes equations along the stagnation streamline of a sphere. According to the results by William et al. [6], the shock standoff distance at the stagnation point predicted by the dimensionally reduced quasi 1-D equations is about 10% shorter than that obtained by the original 2-D/axisymmetric equations. This tendency is the same as that shown in the result by Klomfass and Müller [5].

In this study, a computational procedure to solve the flow field along the stagnation streamline of a blunt body in hypersonic flow is suggested. Dimensionally reduced quasi 1-D Navier-Stokes equations are solved by applying the implicit finite volume method. The computational domain is confined from the stagnation point to a shock wave, and the shock fitting method is used to find the shock position. The boundary condition at the shock is proposed, which employs the shock wave angle in the vicinity of the stagnation streamline using the shock shape correlation by Billig [7]. Numerical computations are conducted for hypersonic flow over a sphere to assess the accuracy of the quasi 1-D Navier-Stokes code. Results such as the flow properties along the stagnation streamline, the shock standoff distance, and the stagnation point heat flux produced by the quasi 1-D Navier-Stokes code are compared with those obtained by the 2-D/axisymmetric Navier-Stokes code and experiment.

2. Governing Equations and Boundary Conditions

2.1 Governing Equations

Navier-Stokes equations in spherical coordinates (r,θ,ϕ) for rotationally symmetric flow $\left(\frac{\partial}{\partial\phi}=0,\ v_\phi=0\right)$ are considered, and the freestream is in the direction of θ=0 as illustrated in Fig. 2. Dimensionally reduced quasi 1-D Navier-Stokes equations are obtained by applying the concept of local similarity used by Kao [3]. Local similarity is achieved by expanding the flow quantities in the powers of the distance from the stagnation point. If we designate the distance as sin θ, the flow quantities are expanded about the axis of symmetry as follows:

$$\begin{aligned}
u(r,\theta) &= u_1(r)\cos\theta + u_2(r)\cos\theta\sin\theta \\
v(r,\theta) &= v_1(r)\sin\theta + v_2(r)\sin^3\theta \\
p(r,\theta) &= p_1(r) + p_2(r)\sin^2\theta + p_3(r)\sin^4\theta \\
\rho(r,\theta) &= \rho_1(r) + \rho_2(r)\sin^2\theta \\
T(r,\theta) &= T_1(r) + T_2(r)\sin^2\theta \\
\mu(r,\theta) &= \mu_1(r) + \mu_2(r)\sin^2\theta
\end{aligned} \tag{1}$$

Here, u is velocity in the radial direction, v is velocity in the tangential direction, p is pressure, ρ is density, T is temperature, and μ is viscosity. In the above, only the terms corresponding to the first truncation are preserved, while for the pressure, p_2 is included in the first truncation [3] as indicated by the dotted line. Substituting the flow quantities of the first truncation into the original Navier-Stokes equations and equating terms that contain similar powers of sin θ, yields a system of equations. In the final step, the equations for the stagnation streamline are specified by letting $\theta \to 0$.

The conservative form of the quasi 1-D Navier-Stokes equations for the analysis of the stagnation line of a spherical body is given as [5, 6]

$$\frac{\partial \boldsymbol{Q}}{\partial t} + \frac{\partial \boldsymbol{F}}{\partial r} - \frac{\partial \boldsymbol{F}_v}{\partial r} + \frac{1}{r}(\boldsymbol{G} - \boldsymbol{G}_v) = 0 \tag{2}$$

Here, the components of conserved variables vector Q, the inviscid flux vectors F and G, and the viscous flux vectors F_v, and G_v are given as follows:

$$\boldsymbol{Q} = \begin{bmatrix} \rho_1 \\ \rho_1 u_1 \\ \rho_1 v_1 \\ \rho_1 E \end{bmatrix} \quad \boldsymbol{F} = \begin{bmatrix} \rho_1 u_1 \\ \rho_1 u_1^2 + p_1 \\ \rho_1 u_1 v_1 \\ \rho_1 u_1 H \end{bmatrix} \quad \boldsymbol{F}_v = \begin{bmatrix} 0 \\ \tau_{rr} \\ \tau_{r\theta} \\ u_1\tau_{rr} - q_r \end{bmatrix}$$
$$\boldsymbol{G} = \begin{bmatrix} 2\rho_1(u_1+v_1) \\ 2\rho_1 u_1(u_1+v_1) \\ 3\rho_1 v_1(u_1+v_1) + 2p_2 \\ 2\rho_1(u_1+v_1)H \end{bmatrix} \quad \boldsymbol{G}_v = \begin{bmatrix} 0 \\ 2(\tau_{rr}+\tau_{r\theta}-2\tau_{\theta\theta}) \\ 3\tau_{r\theta}-\tau_{\theta\theta} \\ 2(u_1\tau_{rr}+u_1\tau_{r\theta}+v_1\tau_{\theta\theta}-q_r) \end{bmatrix} \tag{3}$$

where the viscous stresses and heat flux are expressed as

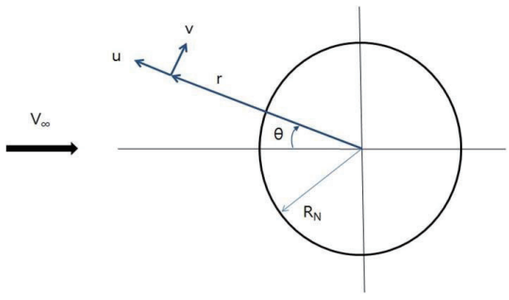

Fig. 2. Coordinate system.

DOI: http://dx.doi.org/10.5139/IJASS.2016.17.2.149

$$\tau_{rr} = \frac{M_\infty}{Re_\infty}\mu_1\left(\frac{4}{3}\frac{\partial u_1}{\partial r} - \frac{4}{3}\frac{u_1+v_1}{r}\right)$$

$$\tau_{\theta\theta} = \frac{M_\infty}{Re_\infty}\mu_1\left(-\frac{2}{3}\frac{\partial u_1}{\partial r} + \frac{2}{3}\frac{u_1+v_1}{r}\right) \quad (4)$$

$$\tau_{r\theta} = \frac{M_\infty}{Re_\infty}\mu_1\left(\frac{\partial v_1}{\partial r} - \frac{u_1+v_1}{r}\right)$$

$$q_r = -\frac{M_\infty}{Re_\infty}\frac{\mu_1}{\Pr(\gamma-1)}\frac{\partial T_1}{\partial r}$$

Pressure p_1 is determined by the equation of state as follows,

$$p_1 = (\gamma - 1)\left(\rho_1 E - \frac{1}{2}\rho_1 u_1^2\right) \quad (5)$$

where E is the specific total energy, and the specific total enthalpy H is expressed as

$$H = E + \frac{p_1}{\rho_1} \quad (6)$$

We need an additional equation for pressure. Pressure p_2 in the θ momentum equation is obtained from the radial momentum equation developed at the second order in θ by neglecting the viscous terms [3, 6]

$$\frac{d}{dr}(p_1 + p_2) = \frac{\rho_1 v_1}{r}(u_1 + v_1) \quad (7)$$

2.2 Boundary Conditions

At the stagnation point, the conditions of no-slip, constant wall temperature, and zero pressure gradient are imposed as follows:

$$u_1 = 0 \qquad v_1 = 0 \qquad T_1 = T_{wall} \qquad \frac{dp_1}{dr} = 0 \quad (8)$$

The other boundary of the computational domain is the shock wave. In previous research [5], the normal shock wave is assumed at the shock boundary, and velocities u_1 and v_1 are imposed as follows:

$$u_1 = u_\infty \qquad v_1 = u_\infty$$

While this boundary condition means θ=0, this assumption is not adequate for the concept of deriving the governing equations for the stagnation streamline, which implies $\theta \to 0$. We suggest that the shock boundary condition is imposed at the position of (x_s, y_s), which corresponds to the small value of θ instead of the intersection point between the shock and stagnation streamline (Fig. 3) [8]. The flow quantities behind the shock wave inclined to the freestream are then obtained using the Rankine-Hugoniot relations.

The shock wave angle is calculated as [9]

$$\theta_s = \theta_b + \tan^{-1}\left(\frac{1}{1+\delta}\frac{d\delta}{d\theta}\right) \quad (9)$$

where θ_s is the tangential angle at the shock, θ_b is the tangential angle at the body θ_b=π/2-θ_1, and δ is the shock standoff distance at the stagnation line. The derivative of the shock standoff distance with respect to θ is numerically approximated as follows:

$$\frac{d\delta}{d\theta} \approx \frac{\Delta\delta}{\Delta\theta} = \frac{\delta_1 - \delta}{\theta_1} \quad (10)$$

where θ_1 is a numerically small value. In addition, δ_1 is the shock standoff distance at the angle θ_1, and can be calculated from the distance between the point at the shock (x_s, y_s) and the point at the body (x_b, y_b), as

$$\delta_1 = \sqrt{(x_s - x_b)^2 + (y_s - y_b)^2} \quad (11)$$

The coordinate of position (x_s, y_s) is calculated with the formula by Billig [7], which depicts the shock shape for a blunt body as

$$x = 1 + \delta - \frac{R_s}{\tan^2\beta}\sqrt{1 + \frac{y^2\tan^2\beta}{R_s^2}} + \frac{R_s}{\tan^2\beta} \quad (12)$$

where x, y are the coordinates of the shock wave, R_s is the radius of curvature of the shock, and β is the wave angle. For a sphere, δ and R_s are calculated as

$$\delta = 0.143\exp\left(3.24/M_\infty^2\right) \quad (13)$$

$$R_s = 1.143\exp\left[0.54/\left(M_\infty - 1\right)^{1.2}\right] \quad (14)$$

Also, for the angle of θ_1, the line in the radial direction with a slope of a=tan θ_1 is given as

$$y = a\,x \quad (15)$$

Thus, we can obtain the coordinate of the point at the shock (x_s, y_s) using Eq. (12) and Eq. (15). The initial value of the shock distance at the stagnation line is obtained from Eq. (13) after the first iteration δ has been calculated from

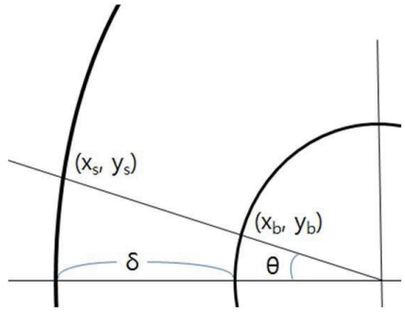

Fig. 3. Notations used in shock geometry.

the shock fitting algorithm. On the other hand, the radius of curvature of the shock, R_s, is obtained from Eq. (14) throughout the iterations.

At the shock boundary, the velocity is decomposed into the shock normal and shock tangent components with the shock angle θ_s. The flow quantities behind the shock are calculated by the Rankine-Hugoniot relations for moving shock as follows:

$$\rho_s(u_s - V_s) = \rho_\infty(u_s - V_s) \tag{16}$$

$$\frac{\rho_s}{\rho_\infty} = \frac{(\gamma+1)M_{n\infty}^2}{(\gamma-1)M_{n\infty}^2+2} \tag{17}$$

$$\frac{p_s}{p_\infty} = 1 + \frac{2\gamma(M_{n\infty}^2-1)}{\gamma+1} \tag{18}$$

where

$$M_{n\infty} = \frac{u_\infty - V_s}{a_\infty} \tag{19}$$

In the above, subscript ∞ means ahead of the shock and subscript s means behind the shock, u and v are the velocity components normal and tangential to the shock, respectively, V_s is the shock velocity, and a is the speed of sound. From these equations, we can obtain the flow quantities behind the shock. With Eq. (1), the boundary condition at the shock wave is given as follows:

$$u_1 = \frac{u_s}{\cos\theta_1} \qquad v_1 = \frac{v_s}{\sin\theta_1} \qquad p_1 = p_s \qquad \rho_1 = \rho_s \tag{20}$$

3. Numerical Procedures

3.1 Spatial Discretization and Time Integration

Eq. (2) is transformed into a generalized coordinate η. Using a finite volume method, we obtain the following semidiscrete conservation approximation at a cell i with unit spacing $\Delta\eta$=1:

$$\left(\frac{1}{J}\frac{\partial \boldsymbol{Q}}{\partial t}\right)_i + \left(\widetilde{\boldsymbol{F}} - \widetilde{\boldsymbol{F}}_v\right)_{i+\frac{1}{2}} - \left(\widetilde{\boldsymbol{F}} - \widetilde{\boldsymbol{F}}_v\right)_{i-\frac{1}{2}} + \left[\frac{1}{Jr}(\boldsymbol{G} - \boldsymbol{G}_v)\right]_i = 0 \tag{21}$$

where subscript 1/2 means the interface of the cell and J is the Jacobian of the coordinate transformation. The ~ symbol denotes the numerically approximated flux at the cell interface. Eq. (21) provides a set of coupled ordinary differential equations with respect to time. The application of the implicit Euler backward scheme and the time linearization of the nonlinear terms result in

$$\left[\frac{\boldsymbol{I}}{J\Delta t} + \left(\frac{\partial \boldsymbol{R}}{\partial \boldsymbol{Q}}\right)^{\mathrm{n}}\right]\Delta \boldsymbol{Q}^{\mathrm{n}} = -\boldsymbol{R}^{\mathrm{n}}(\boldsymbol{Q}) \tag{22}$$

where the residual vector is given as

$$\boldsymbol{R}(\boldsymbol{Q}) = \left(\widetilde{\boldsymbol{F}} - \widetilde{\boldsymbol{F}}_v\right)_{i+\frac{1}{2}} - \left(\widetilde{\boldsymbol{F}} - \widetilde{\boldsymbol{F}}_v\right)_{i-\frac{1}{2}} + \left[\frac{1}{Jr}(\boldsymbol{G} - \boldsymbol{G}_v)\right]_i \tag{23}$$

For the calculation of inviscid numerical flux, $\widetilde{\boldsymbol{F}}_{1/2}$, a modified low-diffusion flux-splitting scheme [10] is used. High order accuracy in space is achieved with the Monotonic Upwind Scheme for Conservation Laws (MUSCL) approach [11]; the primitive variables (ρ,u,v,p) are extrapolated to the cell interface with the minmod limiter function. The viscous flux is discretized by central difference. For the calculation of Jacobian matrices, $\partial R/\partial Q$ in the implicit part, the first-order Steger-Warming's flux vector splitting scheme [12] is used for inviscid flux and the treatment by Tysinger et al. [13] is used for viscous flux.

The residual vector at point i in the implicit part is dependent on the states of the two neighboring grid points. The resulting matrix equation can be written as

$$\mathbf{C}_1\Delta\boldsymbol{Q}_i^{\mathrm{n}} + \mathbf{C}_2\Delta\boldsymbol{Q}_{i-1}^{\mathrm{n}} + \mathbf{C}_3\Delta\boldsymbol{Q}_{i+1}^{\mathrm{n}} = -\boldsymbol{R}_i^{\mathrm{n}} \tag{24}$$

Coefficient matrices composed of inviscid flux Jacobian ($\boldsymbol{A}^{\pm} = \boldsymbol{X}^{-1}\boldsymbol{\Lambda}^{\pm}\boldsymbol{X}, \boldsymbol{B} = \partial \boldsymbol{G}/\partial \boldsymbol{Q}$) and viscous flux Jacobian ($\boldsymbol{A}_{v2} = \partial \boldsymbol{F}_v/\partial \boldsymbol{Q}_\eta$) are given as

$$\begin{aligned}
\mathbf{C}_1 &= \boldsymbol{A}_i^{+} - \boldsymbol{A}_i^{-} + J_{i+\frac{1}{2}}\boldsymbol{A}_{v2_i} + J_{\mathrm{i}-\frac{1}{2}}\boldsymbol{A}_{v2_i} + \left(\frac{B}{Jr}\right)_i \\
\mathbf{C}_2 &= -\boldsymbol{A}_{i-1}^{+} - J_{i-\frac{1}{2}}\boldsymbol{A}_{v2_{i-1}} \\
\mathbf{C}_3 &= \boldsymbol{A}_{i+1}^{+} - J_{i+\frac{1}{2}}\boldsymbol{A}_{v2_{i+1}}
\end{aligned} \tag{25}$$

ΔQ^n can be obtained by solving a block tridiagonal matrix equation. The conserved variable vector at the $(n+1)th$ time level is then finally updated as

$$\boldsymbol{Q}^{\mathrm{n}+1} = \boldsymbol{Q}^{\mathrm{n}} + \Delta\boldsymbol{Q}^{\mathrm{n}} \tag{26}$$

3.2 Shock Fitting Method

Rawat and Zhong [14] conducted evaluations of various shock fitting algorithms for shock-turbulence interaction problems. Among these evaluations, the shock fitting method developed by Henrick et al. [15] is employed in this study. This method uses the momentum equation along the shock normal direction instead of a characteristic relation. The momentum normal to the shock wave is obtained by using the Rankine-Hugoniot relations as

$$\rho_s u_s = \frac{\rho_\infty(V_s-u_\infty)\left[\rho_\infty u_\infty\gamma\left(V_s-u_\infty\right)-2\gamma p_\infty+\rho_\infty(2V_s^2-3V_s u_\infty+u_\infty^2)\right]}{2\gamma p_\infty+\gamma\rho_\infty\left(V_s-u_\infty\right)^2-\rho_\infty\left(V_s-u_\infty\right)^2} \tag{27}$$

The momentum is only a function of shock velocity V_s, and

shock acceleration can be written as the chain rule as follows

$$\frac{dV_s}{dt} = \left[\frac{d(\rho_s u_s)}{dV_s}\right]^{-1} \frac{d(\rho_s u_s)}{dt} \tag{28}$$

The derivative of the momentum with respect to the shock velocity is obtained from Eq. (27) and the term $d(\rho_s u_s)/dt$ is computed from the momentum equation while neglecting viscous terms as

$$\frac{d(\rho_s u_s)}{dt} = -\left[\frac{d(\rho_1 u_1^2 + p_1)}{dr}\right]_s - \frac{2}{r}\rho_{1s} u_{1s}(u_{1s} + v_{1s}) \tag{29}$$

The shock velocity is then calculated from Eq. (28). The location of the shock is obtained from the shock velocity and the grid is modified to follow the new position of the shock at every time step.

4. Results and Discussions

The test case is a hypersonic flow over a sphere in calorically perfect gas with R=287J/kgK, γ=1.4. The nose radius of a sphere is 0.02794m. The freestream conditions are M_∞=10.6, T_∞=47.3K and Re_∞=1.1×10^5, and the wall temperature is 294.4K. Viscosity is calculated from Sutherland's law, and a constant Prandtl number of 0.72 is assumed. These conditions correspond to the experimental conditions of Ref. [16].

First, we attempted to find the suitable value of θ_1 in Eq. (10). Calculations are conducted for values of θ_1 1.0, 0.1, 0.01, and 0.001. The number of grid points is 200 for all calculations. Figs. 4(a) and 4(b) show the effect of θ_1 on the prediction of shock standoff distance and heat flux at the stagnation point. As shown in the results, the shock standoff distance and heat flux are almost the same for the variation of θ_1, except for the heat flux at θ_1 of 1.0. Hereafter, θ_1 of 0.01 is used for all calculations. We also tested the effect of the number of grid points on the results. Calculations are performed for four grid points, 100, 200, 400, and 800, and the shock standoff distance and heat flux at the stagnation point are compared in Fig. 5. The influence of the number of grid points on the shock standoff distance is minimal, as shown in Fig. 5(a). On the other hand, the heat flux at the

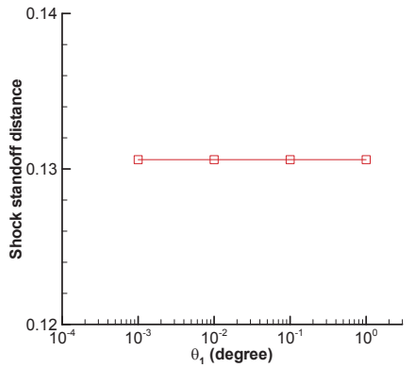

Fig. 4. (a) Effect of θ_1 on shock standoff distance for a sphere at Mach 10.6.

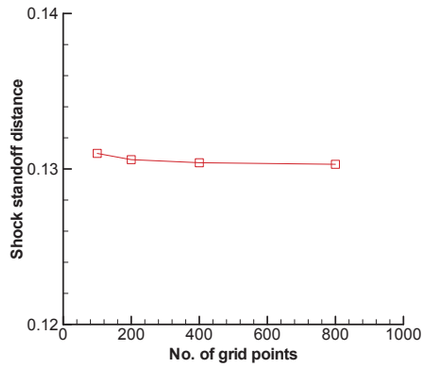

Fig. 5. (a) Effect of the number of grid points on shock standoff distance for a sphere at Mach 10.6.

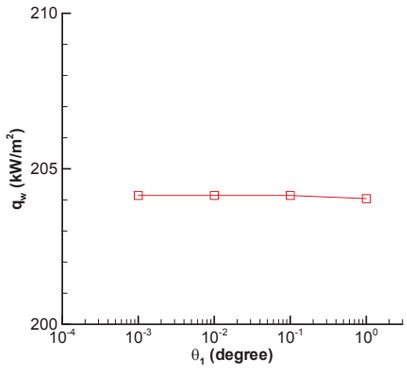

Fig. 4. (b) Effect of θ_1 on stagnation point heat flux for a sphere at Mach 10.6.

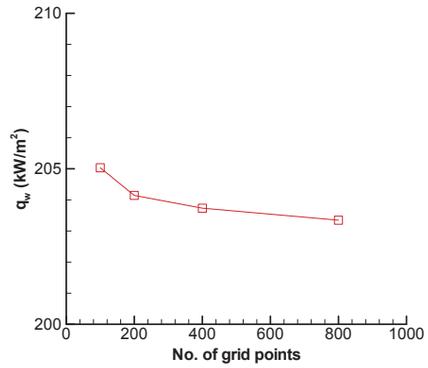

Fig. 5. (b) Effect of the number of grid points on stagnation point heat flux for a sphere at Mach 10.6.

stagnation point decreases as the number of grid points increases, as shown in Fig. 5(b), and the decrement of heat flux is largest when the number of grid points increases from 100 to 200. Through these results, the number of grid points of 200 is used for all calculations of the quasi 1-D code.

Next, the results of the quasi 1-D Navier-Stokes code are validated through comparison with the results of the 2-D/axisymmetric Navier-Stokes code. The 2-D/axisymmetric code [10, 17] employs shock capturing method and has the same numerical algorithms for inviscid flux and time integration as described in the previous chapter. For the 2-D computation, the number of grid points along the body is 120 and normal to the body is 200. Fig. 6 shows pressure contours around a sphere produced by the 2-D/axisymmetric code, and a distinct bow shock is captured without shock instability. For the computations of the quasi 1-D code, freestream conditions are used as initial data and the fixed time step with the Courant-Friedrichs and Lewy (CFL) number of 10 is used. Figs. 7(a), 7(b), and 7(c) show the convergence histories of the density residual, shock velocity, and shock standoff distance, respectively. The shock velocity varies rapidly in the early stage of iteration, and then gradually converges to zero. The profiles of flow

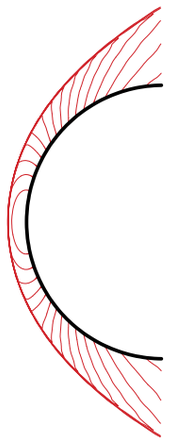

Fig. 6. Pressure contours for a sphere at Mach 10.6.

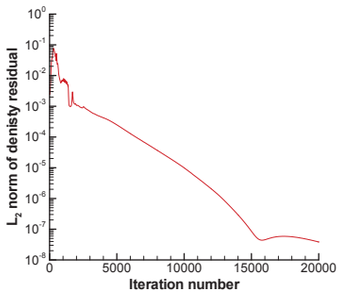

Fig. 7. (a) Convergence history of density residual of quasi 1-D code.

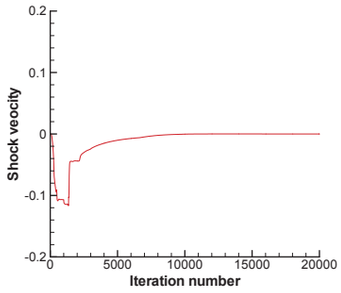

Fig. 7. (b) Convergence history of shock velocity of quasi 1-D code.

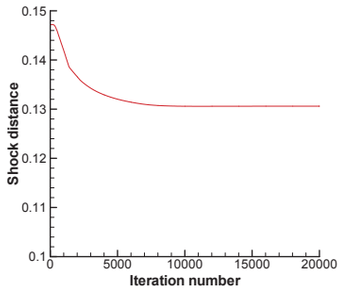

Fig. 7. (c) Convergence history of shock standoff distance of quasi 1-D code.

quantities along the stagnation streamline computed by the quasi 1-D code and 2-D/axisymmetric code are compared in Figs. 8(a) - 8(e). Two results are given for the quasi 1-D code: one using the normal shock boundary condition and the other using the proposed shock boundary condition. In the x axis, the value of 0 refers to the stagnation point and a negative value implies the distance from the stagnation point and terminates at the far field boundary. Distributions of density, pressure, temperature, and Mach number along the stagnation streamline are compared and show excellent agreement. In Fig. 8(e), the pressure profiles near the shock position are enlarged to clearly show the effect of the shock boundary conditions. It can be seen that the shock position predicted by the quasi 1-D code with present shock boundary condition is closer to the shock position by the 2-D/axisymmetric code than that with the normal shock boundary condition. In addition, Fig. 9 shows the comparison of velocities (u_1, v_1) computed by the quasi 1-D code with two boundary conditions at the shock. According to the results, the velocity profiles produced with two boundary conditions slightly differ, and the shock position predicted with the boundary condition of the normal shock wave is shorter than that with the present boundary condition. These results demonstrate that the proposed shock boundary condition improves the prediction capability of the shock position. Fig.

DOI: http://dx.doi.org/10.5139/IJASS.2016.17.2.149

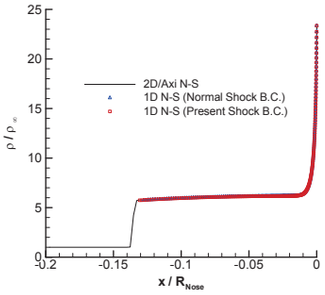

Fig. 8. (a) Comparison of densities along the stagnation streamline of a sphere at Mach 10.6.

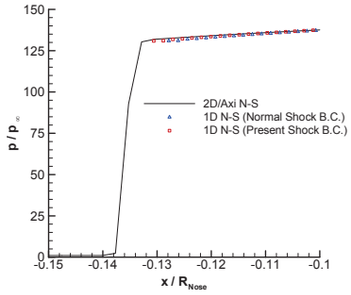

Fig. 8. (e) Enlarged profiles of pressures near the shock wave for a sphere at Mach 10.6.

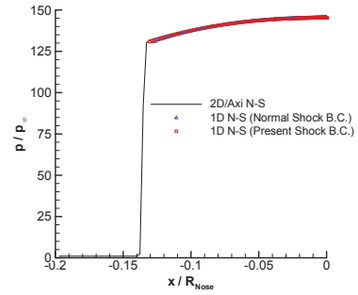

Fig. 8. (b) Comparison of pressures along the stagnation streamline of a sphere at Mach 10.6.

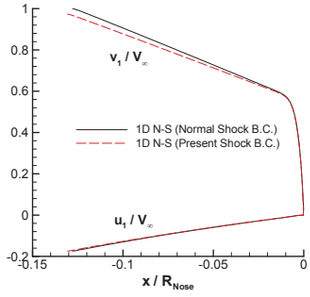

Fig. 9. Effect of shock boundary conditions on velocity profiles along the stagnation streamline.

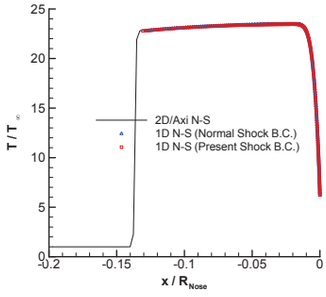

Fig. 8. (c) Comparison of temperatures along the stagnation streamline of a sphere at Mach 10.6.

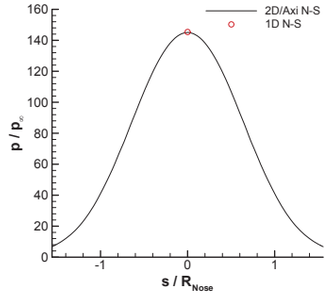

Fig. 10. (a) Comparison of pressures at the stagnation point of a sphere at Mach 10.6.

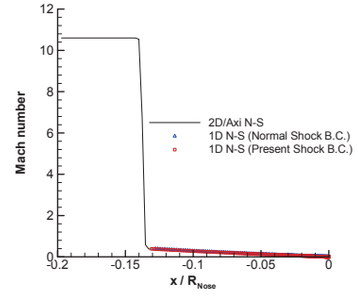

Fig. 8. (d) Comparison of Mach numbers along the stagnation streamline of a sphere at Mach 10.6.

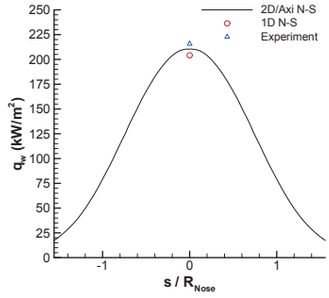

Fig. 10. (b) Comparison of heat fluxes at the stagnation point of a sphere at Mach 10.6.

10(a) shows the wall pressures computed by the two codes, which agree well at the stagnation point. Fig. 10(b) compares the heat fluxes at the stagnation point by the two codes and the experiment [16]. The heat flux predicted by the quasi 1-D code is slightly lower than those obtained by the experiment and the 2-D/axisymmetric code.

5. Conclusion

Numerical computations are conducted for a flow at Mach 10.6 in perfect gas of a sphere by using the quasi 1-D Navier-Stokes equations code. The distributions of flow quantities along the stagnation streamline, the shock standoff distance, and the heat flux at the stagnation point computed by the quasi 1-D code are compared with results obtained by the 2-D Navier-Stokes code and experiment. The proposed shock boundary condition consequently improves the prediction of the shock standoff distance by providing more accuracy. The quasi 1-D code is more efficient in computing time and is more reliable for the flow field analysis along the stagnation streamline and prediction of heat flux at the stagnation point in hypersonic blunt body flows. Also, the quasi 1-D code will be useful for the prediction of heat flux at the stagnation point of a vehicle along the flight trajectory and for the examination of thermo-chemical models if numerical procedures are extended to thermochemical non-equilibrium flow.

References

[1] Fay, J. A. and Riddell, F. R., "Theory of Stagnation Point Heat Transfer in Dissociated Air", *Journal of the Aeronautical Sciences*, Vol. 25, No. 2, 1958, pp. 73-85.

[2] Moretti, G. and Abbett, M., "A Time-Dependent Computational Method for Blunt Body Flows", *AIAA Journal*, Vol. 4, No. 12, 1966, pp. 2136-2141.

[3] Kao, H. C., "Hypersonic Viscous Flow near the Stagnation Streamline of a Blunt Body: I. A Test of Local Similarity", *AIAA Journal*, Vol. 2, No. 11, 1964, pp. 1892-1897.

[4] Jain, A. C. and Adimurthy, V., "Hypersonic Merged Stagnation Shock Layers Part I: Adiabatic Wall Case", *AIAA Journal*, Vol. 12, No. 3, 1974, pp. 342-347.

[5] Klomfass, A. and Müller, S., "Calculation of a Stagnation Streamline Quantities in Hypersonic Blunt Body Flows", *Shock Waves*, Vol. 7, 1997, pp. 12-23.

[6] William, J., Verant, J. and Sagnier, P., "An Efficient Numerical Tool for Blunted Bodies Stagnation Line Rebuilding with Weakly Ionized Thermochemical Nonquilibrium flows", *15th IMACS-World Congress on Scientific Computation, Modeling and Applied Mathematics*, Vol. 3, 1997, pp. 187-192.

[7] Billig, F. S., "Shock Wave Shapes around Spherical and Cylindrical Nosed Bodies", *Journal of Spacecraft and Rockets*, Vol. 4, No. 6, 1967, pp. 822-823.

[8] Lee, C. H., "Numerical Solution of Hypersonic Flow along the Stagnation Streamline of Blunt Body", *The 2015 World Congress on Aeronautics, Nano, Bio, Robotics, and Energy*, Incheon, Korea, August, 2015.

[9] Anderson, E. C. and Moss, J. N., "Numerical Solution of the Hypersonic Viscous Shock Layer Equations for Laminar, Transitional, and Turbulent Flows of a Perfect Gas over Blunt Axially Symmetric Bodies", *NASA TN D-7865*, 1975.

[10] Lee, C. H. and Park, S. O., "Computations of Hypersonic Flows over Blunt Body using a Modified Low-Diffusion Flux-Splitting Scheme", *CFD Journal*, Vol. 10, No. 4, 2002, pp. 490-500.

[11] Anderson, W. K., Thomas, J. L. and Van Leer, B., "Comparison of Finite Volume Flux Vector Splitting for the Euler equations", *AIAA Journal*, Vol. 24, No. 9, 1986, pp. 1453-1460.

[12] Steger, J. L. and Warming, R. F., "Flux Vector Splitting of the Inviscid Gas dynamics Equations with Application to Finite Difference Methods", *Journal of Computational Physics*, Vol. 40, No. 2, 1981, pp. 263-293.

[13] Tysinger, T. L. and Caughy, D. A., "Implicit Multigrid Algorithm for the Navier-Stokes Equations", *AIAA Paper 91-0242*, 1991.

[14] Rawat, P. S. and Zhong, X., "On High-Order Shock Fitting and Front Tracking Schemes for Numerical Simulation of Shock Disturbance Interactions", *Journal of Computational Physics*, Vol. 229, No. 19, 2010, pp. 6744-6780.

[15] Henrick, A. K., Aslam, T. D. and Powers, J. P., "Simulations of Pulsating One-Dimensional Detonations with True Fifth Order Accuracy", *Journal of Computational Physics*, Vol. 213, No. 1, 2006, pp. 311-329.

[16] Cleary, J. W., "Effects of Angle of Attack and Bluntness on Laminar Heating-Rate Distributions of a 15° Cone at a Mach Number of 10.6", *NASA TN D-5450*, 1969.

[17] Lee, C. H. and Park, S. O., "Comparison of Time Implicit Symmetric Gauss-Seidel Iterative Schemes for Computation of Hypersonic Nonequilibrium Flow", *KSAS International Journal*, Vol. 2, No. 1, 2001, pp. 1-11.

DOI: http://dx.doi.org/10.5139/IJASS.2016.17.2.149